Available online at www.sciencedirect.com
SCIENCE DIRECT®
International Journal of Heat and Mass Transfer 48 (2005) 1350–1360
International Journal of HEAT and MASS TRANSFER
www.elsevier.com/locate/ijhmt

On the similarity between gravity and magneto-gravity convection within a non-electroconducting fluid in a differentially heated rectangular cavity

F. Khaldi [a,*], J. Noudem [b], P. Gillon [c]

[a] Laboratoire EPM-MADYLAM, C.N.R.S. B.P. 95, St Martin d'Hères 38402, France
[b] CRISMAT-ISMRA, 6 Bd Maréchal Juin, Caen Cedex 14050, France
[c] LCSR-CNRS, 1C Avenue de la Recherche Scientifique, 45071 Orléans Cedex 2, France

Received 2 February 2004; received in revised form 29 September 2004
Available online 25 December 2004

Abstract

The magneto-gravity convection induced by a vertical magnetic field gradient applied to a non-electroconducting paramagnetic liquid in a differentially heated rectangular cavity is investigated numerically and experimentally. Due to the magnetic susceptibility temperature dependence of the fluid, the magnetic body force drives a thermoconvective motion in the cavity. Depending on the sign of the magnetic gradient, the vertical magnetic force in the liquid can be parallel or antiparallel to gravity. Hence, buoyancy convection in the cavity results of the combination of the vertical magnetic force and of gravity.

Expressed in terms of *Nu* versus *Ra*, the experimental and numerical results are compared to the correlation obtained by Catton without magnetic field. Agreement between the two curves clearly points out the similarity between gravity induced convection and magneto-gravity convection.

1. Introduction

Fluid motions induced by gravity convection render difficult the scientific examination of fundamental phenomena in numerous situations. Different means, often expensive, have been used to damp, even to stop convection, allowing for instance, an access to capillary effects, to improve the understanding of combustion and to grow crystals of better structural quality.

On the other hand, there are situations in which convection has to be enhanced for example to sustain combustion of diffusion flames in space.

Among others, magnetic fields could be a candidate for acting on convection. Numerous studies have been devoted to the action of a magnetic field on convection beginning by the pioneer work of Chandrasekhar [1], based on the Lorentz force which develops in moving electroconducting liquids. Here, we deal with non-conducting materials and base our work on the interaction of the magnetic field with the magnetic property of the fluid.

Magneto-convection induced by moderate magnetic fields (of the order of magnitude of 10–100 G) has been studied in magnetic fluids [2–4] whose magnetic

* Corresponding author.

0017-9310/$ - see front matter © 2004 Elsevier Ltd. All rights reserved.
doi:10.1016/j.ijheatmasstransfer.2004.10.007

Nomenclature

A_y	spanwise aspect ratio, D/L
A_z	vertical aspect ratio, H/L
B	magnetic induction (T)
D	depth of cavity (m)
$\boldsymbol{f}_m$	magnetic force (N/m^3)
$\boldsymbol{g}_m$	terrestrial gravity (m/s^2)
$\boldsymbol{g}_m$	vertical magnetic mass force (m/s^2)
H	height of cavity (m)
k	thermal conductivity (W K^{-1} m^{-1})
L	width of cavity (m)
N	$\frac{\beta_\rho+\beta_\chi}{\beta_\rho}$
n_x	$\frac{\partial B^2/\partial x}{\partial B^2/\partial z}$
n_y	$\frac{\partial B^2/\partial y}{\partial B^2/\partial z}$
Nu	Nusselt number
p	pressure (Pa)
Pr	Prandtl number
q	thermal power (W)
Ra	Rayleigh number
T	temperature (K)
T_c, T_w	cold and warm wall temperature (K)
ΔT	temperature gap, $T_w - T_c$ (K)
T_m	mean temperature, $(T_w + T_c)/2$ (K)
u, v, w	dimensionless velocity in x, y and z directions, respectively
w_{max}	maximum value of w x-profile at $y = 0$ and $z = 0$
w_{gmax}	maximum value of w x-profile at $y = 0$ and $z = 0$ without magnetic field

Greek symbols

α	thermal diffusivity (m^2/s)
β_ρ	thermal expansion coefficient, $-\frac{1}{\rho}\frac{\partial\rho}{\partial T}$ (1/K)
β_χ	relative variation of mass magnetic susceptibility, $-\frac{1}{\chi_m}\frac{\partial\chi_m}{\partial T}$ (1/K)
χ_m	mass magnetic susceptibility (m^3/kg)
δ	thickness of boundary layer (m)
μ_0	vacuum magnetic permeability, $4\times\pi\times10^{-7}$ (H/m)
ν	kinematic viscosity (m^2/s)
θ	dimensionless temperature
ρ	density (kg/m^3)
$\boldsymbol{\pi}$	vertical magneto-gravity buoyancy (N/kg)

Subscripts

0	values at the centre of cavity
c	critical values
m	values at T_m
*	equivalent

susceptibility is about 1. Thermomagnetic convection appears in a ferrofluid submitted to a temperature gradient and a magnetic field gradient due to the fact that the fluid magnetization is temperature dependent.

The development of the superconducting magnet technology allows the control of natural convection by a strong magnetic field gradient in fluids of much lower magnetic susceptibility. Two configurations have been extensively studied in the framework of gravity convection: the cylindrical Rayleigh–Bénard cavity and *the differentially heated rectangular cavity*. The first configuration has been studied by Braithwaite et al. [5] in the air-gap of a vertical superconducting magnet. They have demonstrated that convection within a gadolinium nitrate solution could be magnetically either enhanced or damped. Based on their observations, Huang et al. [6] and Qi et al. [7] have examined theoretically and numerically the mechanism responsible for magneto-gravity thermal convection in the Rayleigh–Bénard configuration. Recently, with the same configuration, Maki et al. [8] evidenced the similarity between gravity convection and magneto-gravity convection induced within air by a vertical magnetic field gradient. The evolution of the Nusselt number versus the Rayleigh number was in agreement with the classical Silveston's correlation (non-magnetic field).

The second configuration: *the differentially heated rectangular cavity* has been investigated in two main experimental studies. In the first one, Carruthers and Wolfe [9] have observed the reversal of convective movements within oxygen gas using an electromagnet, while the aim of the second one, from Seybert et al. [10] was to completely stop the motion driven by thermal convection within a manganese chloride solution using a vertical superconducting magnet. Tagawa et al. [11] have studied numerically the effect of the direction of the magnetic field on natural convection within air in a cubic cavity.

In the present paper, we have studied experimentally and numerically the magneto-gravity convection induced in a cavity with differentially heated sidewalls, filled by a non-electroconducting paramagnetic liquid and set in the bore of a vertical superconducting magnet. The numerical study is three dimensional in order to take into account the three dimensional character of the magnetic field gradient.

The main objective of our investigations, following what has been proven for the cylindrical Rayleigh–Bénard cavity configuration, is to examine if a similarity exists between gravity and magneto-gravity convection in *the differentially heated rectangular cavity configuration*.

We first recall three important relations describing the interaction of a paramagnetic fluid with a magnetic field gradient:

The magnetic body force $\boldsymbol{f}_{\mathrm{m}}$:

$$\boldsymbol{f}_{\mathrm{m}} = \frac{1}{2}\rho(T)\frac{\chi_{\mathrm{m}}(T)}{\mu_0}\nabla B^2, \tag{1}$$

the vertical mass force $\boldsymbol{g}_{\mathrm{m}}$:

$$\boldsymbol{g}_{\mathrm{m}} = \frac{1}{2}\frac{\chi_{\mathrm{m}}(T)}{\mu_0}\frac{\partial B^2}{\partial z}i_z, \tag{2}$$

and Curie's law:

$$\chi_{\mathrm{m}} \propto \frac{1}{T}. \tag{3}$$

2. Experimental

The experimental study is intended to trace the evolution of the magneto-gravity-induced heat transfer in the case where $\boldsymbol{g}_{\mathrm{m}}$ is antiparallel to $\boldsymbol{g}$. The apparatus may be seen Fig. 1. The cavity of dimensions: $L = 8$ mm, D=30 mm and $H = 30$ mm contains a paramagnetic fluid (aqueous solution of nitrate gadolinium with a concentration of 433 kg/m^3 and a magnetic susceptibility $\chi_{\mathrm{m}} = 1.63 \times 10^{-7}$ m^3/kg). One of the side walls is maintained at fixed temperature $T_{\mathrm{c}} = 293$ K by a water circulation, whereas the opposite wall is heated by a Constantan wire resistance. The other walls are made of Plexiglas. A Copper-Constantan thermocouple records the temperature difference between both active copper walls. The cavity is thermally isolated by expanded Polystyrene. For each injected power q, the Nu number is derived from the temperature drop ΔT.

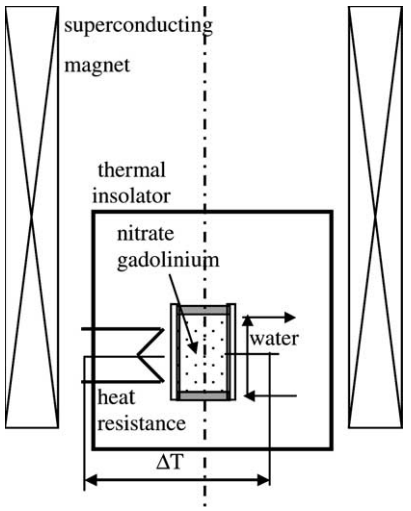

Fig. 1. Schematic of experimental apparatus.

$$Nu = \frac{q/DH}{k\Delta T/L}. \tag{4}$$

The experiments were carried out in the air-gap of a superconducting magnet delivering an axisymmetric vertical magnetic field. The cavity is centered on the magnet axis; at 110 mm below the magnet centre. The evolution of Nu is measured according to the magnetic field gradient intensity for 4 values of ΔT: 5, 10, 15 and 20 K.

3. Numerical analysis

In addition to the experimental conditions, the numerical study analyses also the case where $\boldsymbol{g}$ and $\boldsymbol{g}_{\mathrm{m}}$ are parallel. The numerical model is depicted in Fig. 2. The cavity has $A_y = A_z = 3.75$. The warm wall (left) is maintained at T_{w} whereas the cold (right) one is maintained at T_{c}. All the other walls of the cavity are supposed adiabatic. The thermophysical properties of the liquid are supposed the same that those of water and their values are taken at temperature T_{m}. The flow within the cavity is assumed stationary, laminar, incompressible and Newtonian. The Boussinesq approximation holds.

We have used the semi-analytical method proposed by Urankar [12] to calculate $\partial B^2/\partial z$ and $\partial B^2/\partial r$, the vertical and the radial component of ∇B^2. In the volume of the cavity, $\partial B^2/\partial r$ is projected in two components, transversal $\partial B^2/\partial x$, and spanwise $\partial B^2/\partial y$. In Fig. 3, are traced

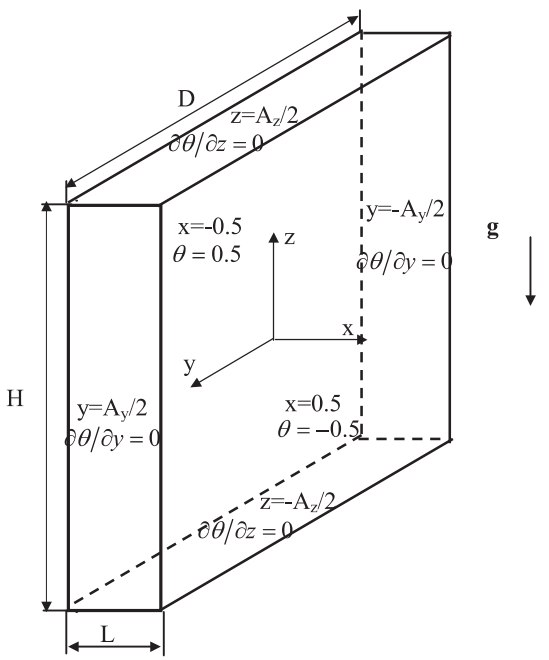

Fig. 2. Computational domain and dimensionless boundary conditions.

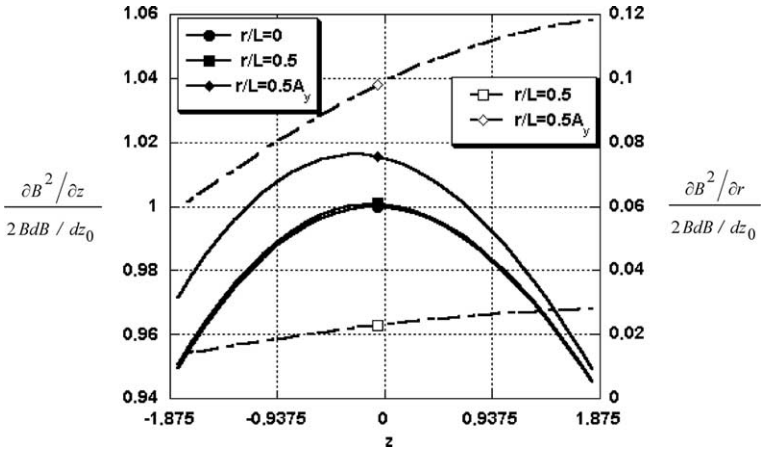

Fig. 3. Vertical profiles of $\partial B^2/\partial z$ and $\partial B^2/\partial r$, closed and opened symbols, respectively, normalized to $2B\mathrm{d}B/\mathrm{d}z_0$.

vertical profiles of $\partial B^2/\partial z$ and $\partial B^2/\partial r$ normalized to $2B\mathrm{d}B/\mathrm{d}z_0$ which represents the value of $\partial B^2/\partial z$ at the centre of the cavity. It is seen that the two $\partial B^2/\partial z$ profiles along the axis of the magnet (i.e. $r/L = 0$) and along the two isothermal active walls of the cavity ($r/L = 0.5$) coincide and present a vertical homogeneity of 5%. Whereas, along the two vertical adiabatic walls ($r/L = 0.5A_y$), $\partial B^2/\partial z$ is higher, it reaches a maximum (1.5% of $2B\mathrm{d}B/\mathrm{d}z_0$) at the mid-height of the cavity and its profile along y presents a homogeneity of 5%. The radial component $\partial B^2/\partial \mathrm{r}$ is maximal along the two vertical adiabatic cavity walls but remains relatively weak and does not go beyond 12% of $2B\mathrm{d}B/\mathrm{d}z_0$. Fig. 4 presents iso-values, normalized to $2B\mathrm{d}B/\mathrm{d}z_0$, of three components, $\partial B^2/\partial x$, $\partial B^2/\partial y$ and $\partial B^2/\partial z$ in the (x, y) plane at three levels: top, mid-height, and bottom. It is seen that the magnetic buoyancy force is vertical on the axis and three dimensional elsewhere in the cavity with a dominant vertical component. From this result, it is convenient to express the transversal, spanwise and vertical components of the magnetic mass force, respectively:

$$n_x g_\mathrm{m}, n_y g_\mathrm{m}, g_\mathrm{m}, \quad \text{with } n_x = \frac{\partial B^2/\partial x}{\partial B^2/\partial z} \text{ and } n_y = \frac{\partial B^2/\partial y}{\partial B^2/\partial z}. \tag{5}$$

The magnetic field gradient distribution being 3D, we have chosen to develop a 3D numerical study of the flow.

In the adimensionalization, the value of $\boldsymbol{g}_\mathrm{m}$ at the centre of the cavity:

$$g_{\mathrm{m}0} = \frac{\chi_\mathrm{mm}}{\mu_0} B\mathrm{d}B/\mathrm{d}z_0 \tag{6}$$

is taken as a reference of the magnetic force. The width of the cavity L is taken as the reference length for spatial coordinates. Velocity, pressure, temperature and difference temperature references are defined as α/L, $\rho\alpha^2/L^2$, T_m and ΔT, respectively. Also, we have

$$n_{x0} = \frac{\partial B^2/\partial x(x = 0.5, y = 0, z = 0)}{2B\mathrm{d}B/\mathrm{d}z_0} \quad \text{and}$$
$$n_{y0} = \frac{\partial B^2/\partial y(x = 0, y = 0.5A_y, z = 0)}{2B\mathrm{d}B/\mathrm{d}z_0}.$$

Due to the fact that n_{x0} and $n_{y0} \gg 1$, the heat transfer in the cavity is governed mainly by the combined effect of $\boldsymbol{g}$ and $\boldsymbol{g}_{\mathrm{m}0}$. The resulting vertical magneto-gravity force can be expressed as

$$\boldsymbol{\pi} = \rho\beta_\rho \boldsymbol{g} + \rho(\beta_\rho + \beta_\chi)\boldsymbol{g}_{\mathrm{m}0}. \tag{7}$$

Thus, we can introduce an equivalent gravity $\boldsymbol{g}^*$, defined as

$$\boldsymbol{g}^* = \boldsymbol{g}\left(1 + N\frac{\boldsymbol{g}_{\mathrm{m}0}}{\boldsymbol{g}}\right), \tag{8}$$

which is included in the Ra definition as follows:

$$Ra = \frac{\beta_\rho g^* \Delta T L^3}{\nu\alpha} \tag{9}$$

Finally, the heat transfer and flow in the cavity are governed by the laws of conservation of mass, momentum and energy. These equations written in dimensionless forms are as follows:

$$\left.\begin{aligned}
&\frac{\partial u}{\partial x} + \frac{\partial v}{\partial y} + \frac{\partial w}{\partial z} = 0,\\
&u\frac{\partial u}{\partial x} + v\frac{\partial u}{\partial y} + w\frac{\partial u}{\partial z} = -\frac{\partial p}{\partial x} + Pr\left(\frac{\partial^2 u}{\partial x^2} + \frac{\partial^2 u}{\partial y^2} + \frac{\partial^2 u}{\partial z^2}\right) + n_{x0}\frac{g_m}{g^*}NRaPr\theta,\\
&u\frac{\partial v}{\partial x} + v\frac{\partial v}{\partial y} + w\frac{\partial v}{\partial z} = -\frac{\partial p}{\partial y} + Pr\left(\frac{\partial^2 v}{\partial x^2} + \frac{\partial^2 v}{\partial y^2} + \frac{\partial^2 v}{\partial z^2}\right) + n_{y0}\frac{g_m}{g^*}NRaPr\theta,\\
&u\frac{\partial w}{\partial x} + v\frac{\partial w}{\partial y} + w\frac{\partial w}{\partial z} = -\frac{\partial p}{\partial z} + Pr\left(\frac{\partial^2 w}{\partial x^2} + \frac{\partial^2 w}{\partial y^2} + \frac{\partial^2 w}{\partial z^2}\right) + RaPr\theta,\\
&\text{and}\\
&u\frac{\partial \theta}{\partial x} + v\frac{\partial \theta}{\partial y} + w\frac{\partial \theta}{\partial z} = \frac{\partial^2 \theta}{\partial x^2} + \frac{\partial^2 \theta}{\partial y^2} + \frac{\partial^2 \theta}{\partial z^2}.
\end{aligned}\right\} \tag{10}$$

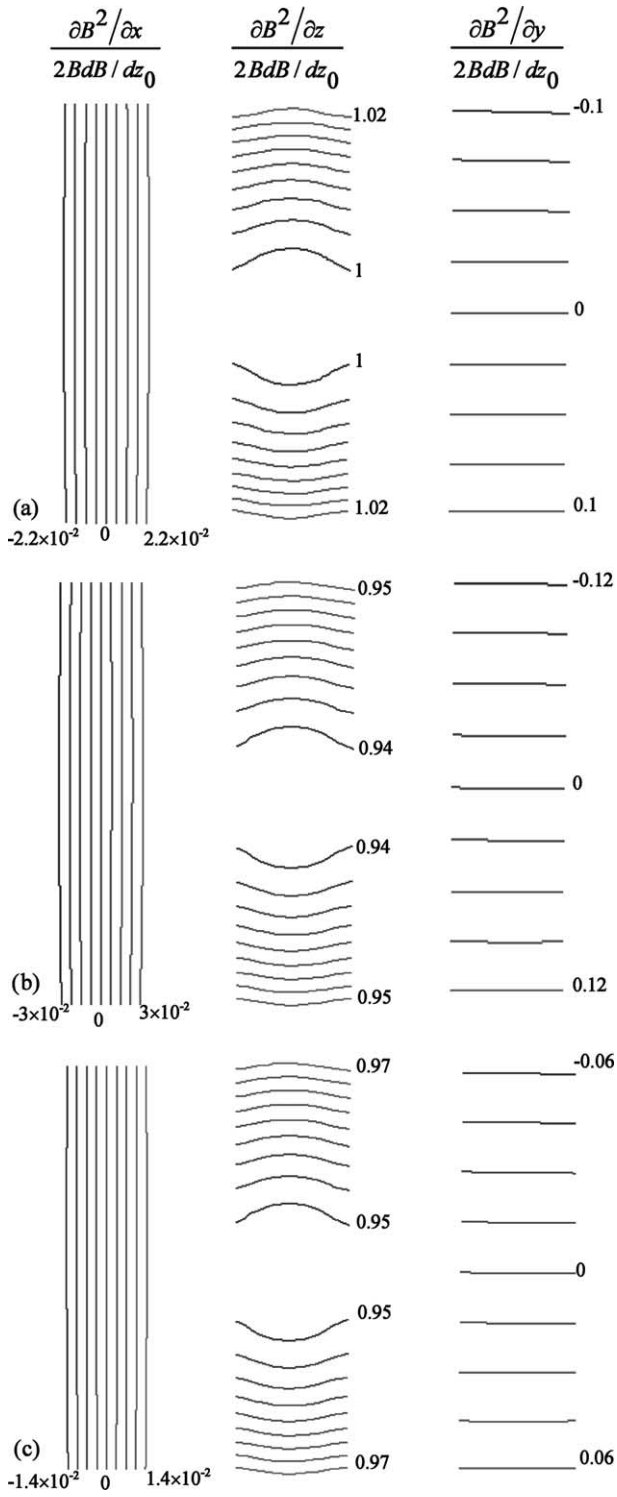

Fig. 4. Iso-values of $\partial B^2/\partial x$, $\partial B^2/\partial y$ and $\partial B^2/\partial z$, normalized to $2B\mathrm{d}B/\mathrm{d}z_0$ at: (a) $z = 0$, (b) $z = A_z/2$ and (c) $z = -A_z/2$.

The numerical resolution of these equations is achieved using the computation code Fluent [13] with the algorithm SIMPLEC. Second order schemes are used to discretize the diffusion and convection terms.

Table 1
Ra values versus positive and negative values of $B\mathrm{d}B/\mathrm{d}z_0$ for the four values of ΔT

BdB/dz_0 (T^2/m) \ ΔT(K)		5	10	15	20
0		4.82	11.4	20.1	31.0
+	4.00	1.28	4.00	8.40	14.7
-		8.36	18.9	31.8	47.3
+	**5.45**	0	1.31	4.16	8.80
-		9.64	21.6	36.0	53.2
+	5.50	0.05	1.20	4.00	86.0
-		9.68	21.6	36.2	53.4
+	6.00	4.02	2.88	2.55	6.53
-		1.01	22.6	37.6	55.5
+	6.15	4.20	0	2.11	5.92
-		10.2	22.8	38.7	56.1
+	6.87	1.26	1.33	0	3.00
-		10.9	24.2	20.1	59.0
+	7.60	1.9	2.68	2.12	0
-		11.5	25.6	42.3	31.0
+	8.00	2.26	3.43	3.29	1.70
-		12.0	26.3	43.5	63.7
+	11.0	4.91	9.00	12.1	13.9
-		14.5	31.9	52.2	75.9

$Ra\times10^4$

After mesh tests, the adopted mesh is composed of $38\times30\times67$ cells in x, y and z directions, respectively. This mesh is non-uniform in the (x, z) plane. For *Ra* above 10^3, three cells are included in the boundary layer along the walls of the cavity. The thickness of this boundary layer is calculated by the formula $\delta = 1.8\times Ra^{-0.25}A_z^{0.25}L$, given by Gill [14]. The mesh expanding ratio is of 1.05. The mesh is uniform in y direction. We conserved enough thin mesh even when the *Ra* number is far less than 10^3. This constraint is imposed by the necessity to ensure the numerical non-rotationally of ∇B^2. Table 1 gives the conditions of the different cases investigated in the present study, *Ra* ranges from 0 to 7.6×10^5.

4. Results and discussion

(a) $\mathbf{g}_m = 0$

In a rectangular cavity with $A_y > 1.7$, McBain [15] verified that the dynamical effects of the two vertical end walls on the flow within the cavity are practically negligible. In the experimental study, we supposed that all non-active walls are perfectly thermally insulated. In fact, it is very difficult to achieve this condition practically, due to the small thermal conductivity ratio between the liquid solution and the Plexiglas walls (~3). In order to characterize the conditions imposed in the experiences as well as at the numerical level, we used the correlation proposed by Catton [16] for the calculation of *Nu* in the absence of magnetic field, according to:

$$Nu = 0.22A_z^{-0.25}\left(\frac{Pr}{0.2+Pr}Ra\right)^{0.28}. \quad (11)$$

Experimental and numerical results obtained at zero magnetic field are compared to Catton's predictions of evolutions of *Nu* versus *Ra* (thus ΔT) in Fig. 5. The values obtained by numerical simulation are very close to the theoretical ones in the range of studied *Ra*; showing a first validation of the numerical model. However, the experimental results deviate from the theory predictions, the difference being more important at greater *Ra* (thus ΔT). We attribute the difference to bad thermal isolation of the walls made in Plexiglas. At higher imposed ΔT, the difference between the mean temperature in the cavity and the ambient temperature is higher too; it induces an increase of the heat losses with increasing ΔT. The relative discrepancy equals 0.4% for $\Delta T = 5$ K and 15% for $\Delta T = 20$ K.

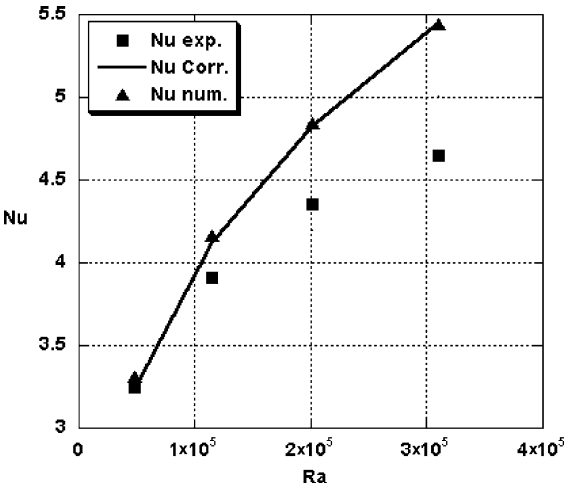

Fig. 5. Evolution of *Nu* versus *Ra* in the absence of magnetic field. Comparisons between experimental (■), obtained from Catton's correlation (full line) and numerical (▲) results.

(b) $\mathbf{g}_m$ antiparallel to $\mathbf{g}$

In this case, gravity and magnetic force are opposed. Fig. 6 presents experimental and numerical variations of *Nu* versus $B\mathrm{d}B/\mathrm{d}z_0$ for $\Delta T = 5$ and 10 K. For $B\mathrm{d}B/\mathrm{d}z_0$ varying between 0 and some critical value designed as $B\mathrm{d}B/\mathrm{d}z_{0c}$, *Nu* decreases from its initial value corresponding to a pure gravity convection regime to a

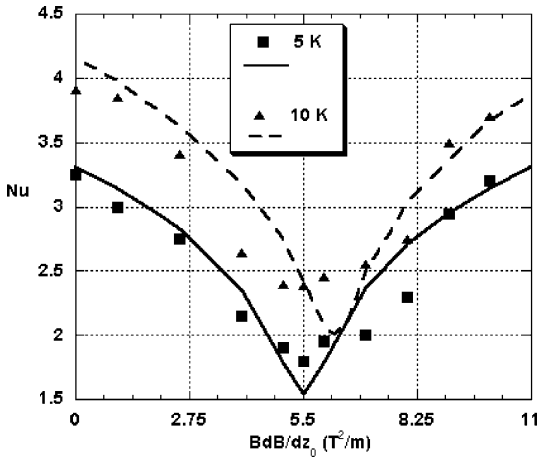

Fig. 6. Evolution of Nu versus $B\mathrm{d}B/\mathrm{d}z_0$, for $\Delta T = 5$ K and $\Delta T = 10$ K. Comparisons between experimental (symbols) and numerical results (lines).

Table 2
Comparisons of $B\mathrm{d}B/\mathrm{d}z_{0c}$ values and Nu minimum values, determined experimentally and numerically for various values of ΔT

ΔT (K)	$B\mathrm{d}B/\mathrm{d}z_{0c}$ (T^2/m)		Nu minimum	
	Experimental results	Numerical results	Experimental results	Numerical results
5	5.50	5.50	1.80	1.54
10	5.50	6.25	2.39	2.01
15	5.50	6.94	2.65	2.39
20	5.50	7.75	2.81	2.67

minimal value for a magneto-gravity regime. The resulting driven force decreases. When $B\mathrm{d}B/\mathrm{d}z_0$ exceeds $B\mathrm{d}B/\mathrm{d}z_{0c}$, Nu increases with $B\mathrm{d}B/\mathrm{d}z_0$ indicating that the heat transfer is accelerated. The magnetic force then stronger than gravity is able to drive the flow motion.

As shown in Table 2, for $\Delta T = 5$ K, $B\mathrm{d}B/\mathrm{d}z_{0c}$ is determined at 5.5 T^2/m by both experiments and numerical simulations. But for the others ΔT, the critical $B\mathrm{d}B/\mathrm{d}z_0$ value is different from experiences and numerical simulation. Here, we discuss the results following the case of $\Delta T = 5$ K without lose of generality. In terms of $\boldsymbol{g}^*$, 5.5 T^2/m corresponds to $\boldsymbol{g}^* \cong 0$ which signifies that vertical magneto-gravity buoyancy is quasi-null. At this value, the w/w_{gmax} x-profile at mid-height of the cavity, presented in Fig. 7 (case (b)), shows a very weak flow velocity ($w/w_{\mathrm{gmax}} < 0.04$) and reveals the loss of its 2D character observed for $B\mathrm{d}B/\mathrm{d}z_0 = 0$ corresponding to $\boldsymbol{g}^* = 1\boldsymbol{g}$ (case (a)). The 3D character is induced by the two horizontal thermomagnetic buoyancies which are revealed due to the quasi-annulation of the vertical

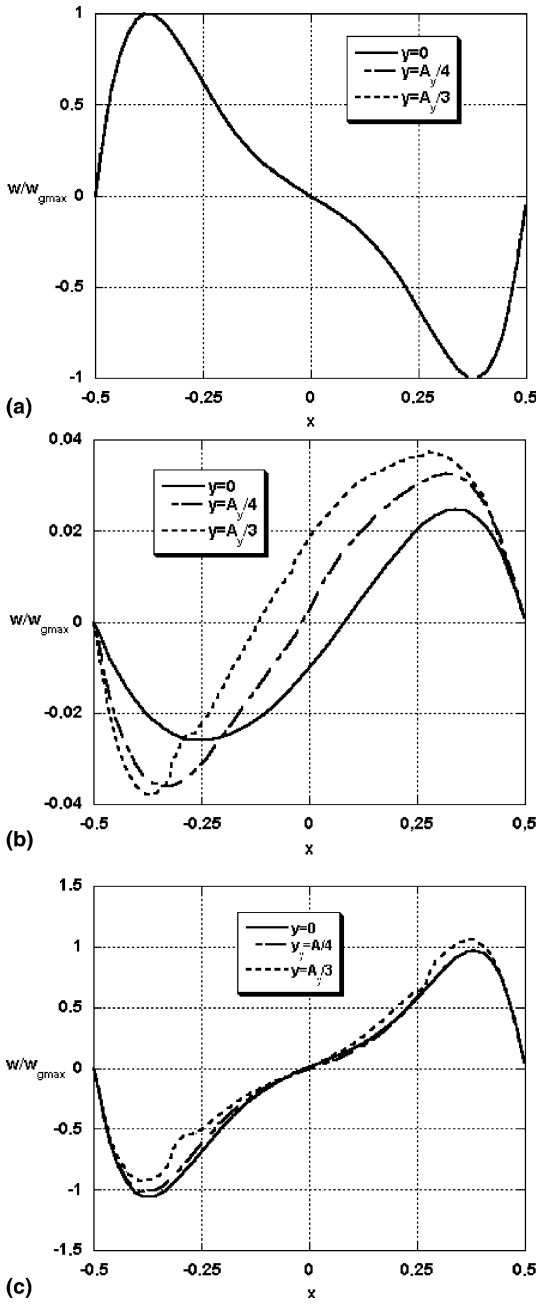

Fig. 7. w/w_{gmax} x-profile at mid-height and mid-depth of the cavity for $\Delta T = 5$ K at: (a) $B\mathrm{d}B/\mathrm{d}z_0 = 0$ T^2/m, (b) $B\mathrm{d}B/\mathrm{d}z_0 = 5.5$ T^2/m and (c) $B\mathrm{d}B/\mathrm{d}z_0 = 11$ T^2/m.

one by the opposed gravity. At the same conditions, the θ x-profile, presented in Fig. 8, reflects a mainly conduction mode of the heat transfer which is convective for $\boldsymbol{g}^* = 1\boldsymbol{g}$. For $B\mathrm{d}B/\mathrm{d}z_0 = 2B\mathrm{d}B/\mathrm{d}z_{0c} = 11$ T^2/m leading to $\boldsymbol{g}^* \cong -1\boldsymbol{g}$, the flow is completely reversed Fig. 7 (case (c)). The corresponding profiles of w/w_{gmax} and θ are

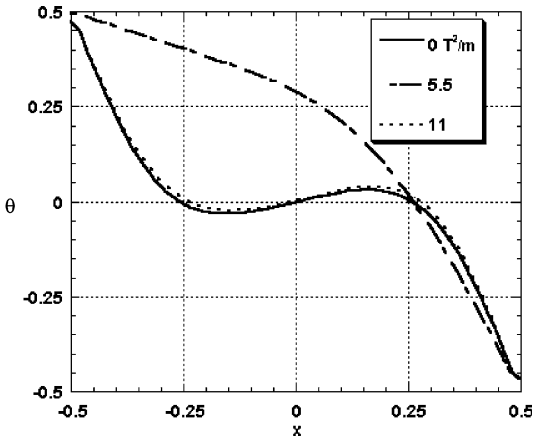

Fig. 8. θ x-profile at mid-height and mid-depth of the cavity for $\Delta T = 5$ K and for various values of $B\mathrm{d}B/\mathrm{d}z_0$.

similar to those for $\boldsymbol{g}^* = 1\boldsymbol{g}$: indeed, they correspond to the same Ra. We observe a slight shift of the identically characteristic of w/w_{gmax} x-profiles which is due to the horizontal thermomagnetic buoyancy whose value increases with $B\mathrm{d}B/\mathrm{d}z_0$.

By numerical simulation $B\mathrm{d}B/\mathrm{d}z_{0c}$ is found to increase with ΔT in agreement with the theoretical predictions, see Table 1 (shaded cells, $Ra = 0$). Whereas in experiences, $B\mathrm{d}B/\mathrm{d}z_{0c}$ is constant for all ΔT due to the non-perfect isolation of the cavity causing the decrease of T_{m} upon which $\boldsymbol{g}^*$ is dependent following *formulas* (2) and (3).

The Nu does not reach 1, as expected theoretically, corresponding to the suppression of convection. The liquid is not entirely stopped everywhere in the cavity due to the non-homogeneity of $B\mathrm{d}B/\mathrm{d}z$ as discussed above. Figs. 9 and 10 show that at $B\mathrm{d}B/\mathrm{d}z_0 = 5.5$ T^2/m (case (b)) the fluid motion is almost stopped with horizontal conductive transfer of heat at the middle of the cavity.

(c) $\boldsymbol{g}_m$ parallel to $\boldsymbol{g}$

In this case, Nu increases with the same tendency for all ΔT while increasing $B\mathrm{d}B/\mathrm{d}z_0$ as shown in Fig. 11.

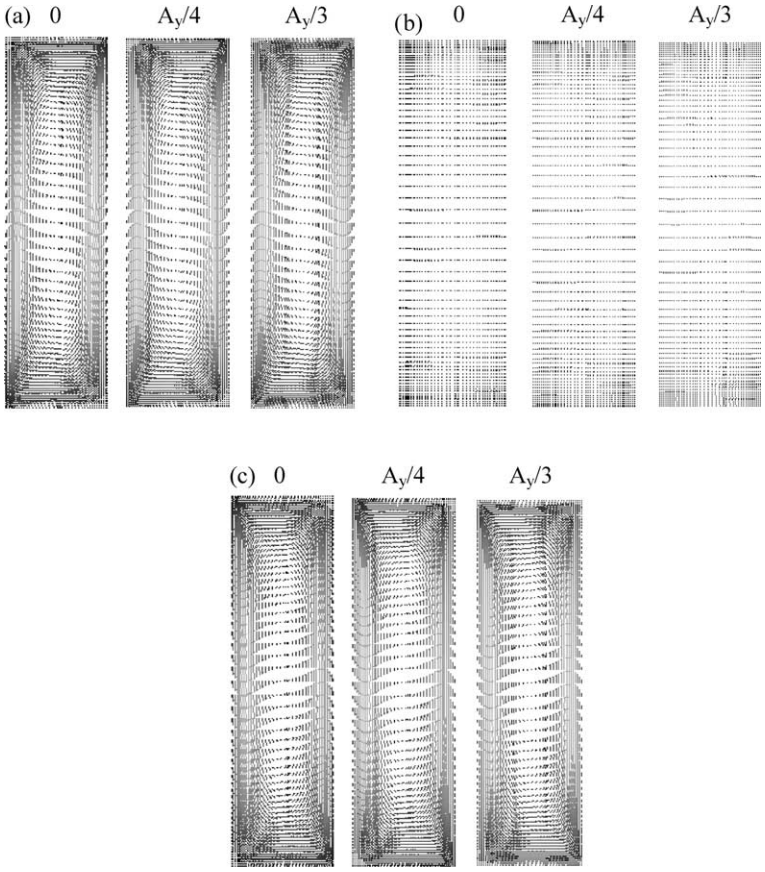

Fig. 9. Velocity field for $\Delta T = 5$ K and for various values of y at: (a) $B\mathrm{d}B/\mathrm{d}z_0 = 0$ T^2/m, (b) $B\mathrm{d}B/\mathrm{d}z_0 = 5.5$ T^2/m and (c) $B\mathrm{d}B/\mathrm{d}z_0 = 11$ T^2/m.

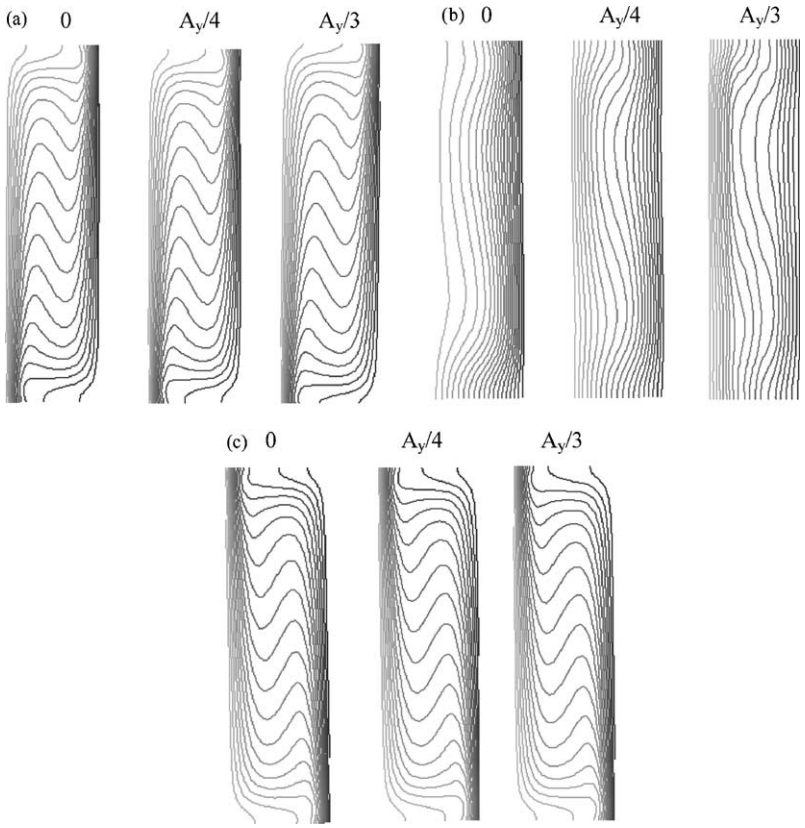

Fig. 10. Isothermal lines for $\Delta T = 5$ K and for various values of y at: (a) $B\mathrm{d}B/\mathrm{d}z_0 = 0$ T^2/m, (b) $B\mathrm{d}B/\mathrm{d}z_0 = 5.5$ T^2/m and (c) $B\mathrm{d}B/\mathrm{d}y_0 = 11$ T^2/m.

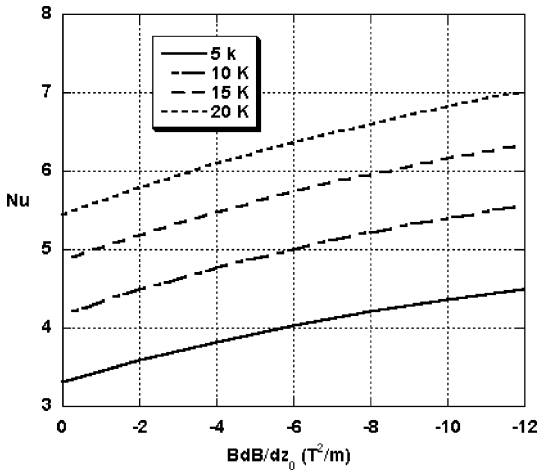

Fig. 11. Numerical Nu evolution versus $B\mathrm{d}B/\mathrm{d}z_0$ for $\Delta T = 5$, 10, 15 and 20 K.

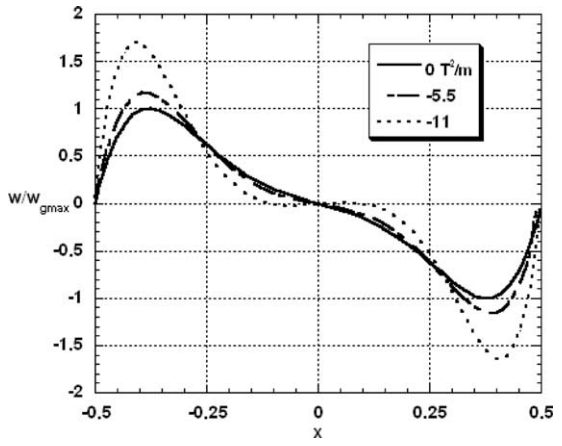

Fig. 12. $w/w_{\max}$ x-profile at mid-height and mid-depth of the cavity for $\Delta T = 5$ K and for various values of $B\mathrm{d}B/\mathrm{d}z_0$.

Figs. 12 and 13 present, respectively, the w/w_{gmax} and x-profiles at mid-height and mid-depth of the cavity for $\Delta T = 5$ K and Fig. 14 presents the $w/w_{\max}$ x-profile at mid-height of the cavity at various depths. These results are for $B\mathrm{d}B/\mathrm{d}z_0 = -5.5$ T^2/m leading to

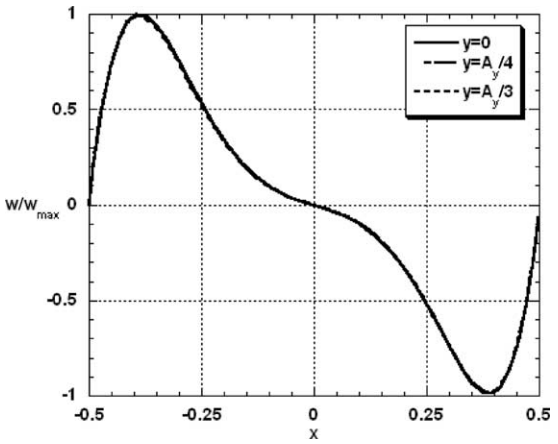

Fig. 13. θ x-profile at mid-height and mid-depth of the cavity for $\Delta T = 5$ K and various values of $B\mathrm{d}B/\mathrm{d}z_0$.

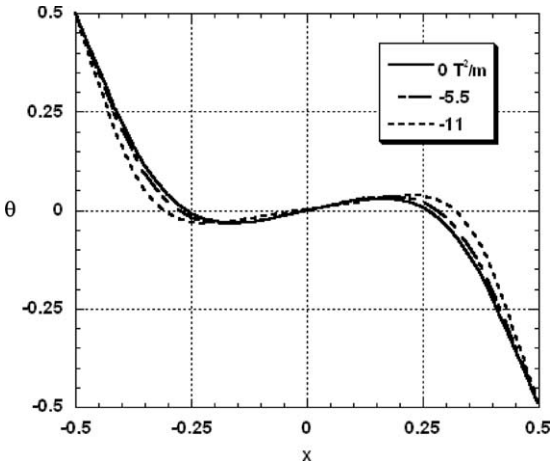

Fig. 14. $w/w_{\max}$ x-profile at mid-height of the cavity for $B\mathrm{d}B/\mathrm{d}z_0 = -5$ T^2/m and various values of y.

$\boldsymbol{g}^* \cong 2\boldsymbol{g}$ and $B\mathrm{d}B/\mathrm{d}z_0 \cong -11$ T^2/m leading to $\boldsymbol{g}^* = 3\boldsymbol{g}$. They are traditional velocity and temperature profiles of intensified 2D convection due to the addition of the two driven forces. The flow velocity increases, the thickness of the boundary layers decreases identically at different depths of the cavity with increasing $B\mathrm{d}B/\mathrm{d}z_0$.

The whole results obtained in the present study are expressed in terms of Nu versus Ra for positive and negative values of $B\mathrm{d}B/\mathrm{d}z_0$, Fig. 15. The experimental and numerical evolutions of magneto-gravity convection are compared to Catton's evolution for pure gravity convection. The agreement between all these evolutions is noticeable. Because Catton's correlation is valid only

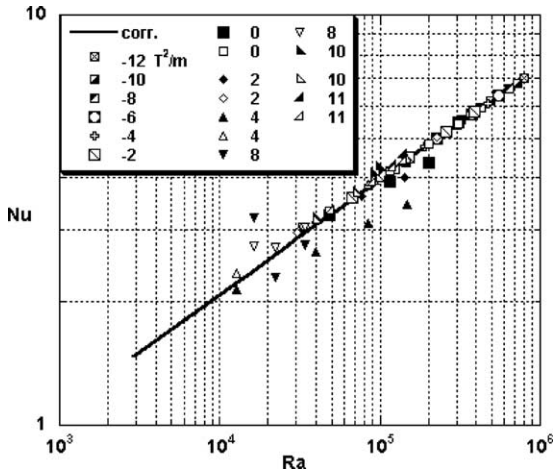

Fig. 15. Experimental (closed symbols) and numerical (opened symbols) Nu versus Ra for various values of $B\mathrm{d}B/\mathrm{d}z_0$, compared to Catton's correlation (full line).

for $Ra > 10^3$; values of $B\mathrm{d}B/\mathrm{d}z_0$ close to $B\mathrm{d}B/\mathrm{d}z_{0c}$ corresponding to small Ra are excluded.

5. Conclusion

We study magneto-gravity thermal convection in a differentially heated rectangular cavity. A vertical magnetic field gradient generates within a non-electroconducting paramagnetic fluid a vertical magnetic force $\boldsymbol{g}_\mathrm{m}$ which can be parallel or antiparallel to gravity $\boldsymbol{g}$. The combination of $\boldsymbol{g}$ and $\boldsymbol{g}_\mathrm{m}$ leads to an equivalent gravity $\boldsymbol{g}^*$ which the motor of vertical magneto-gravity buoyancy convection. After introducing $\boldsymbol{g}^*$ in the Ra definition, the experimental and numerical results expressed in terms of Nu versus Ra, show that heat transfer driven by magneto-gravity buoyancy is similar to that driven by gravity buoyancy only. Therefore, a vertical magnetic field gradient is able to extend the range of Ra at given ΔT. In the present study, a Ra of 4.82×10^4 is reduced to 0 at $B\mathrm{d}B/\mathrm{d}z = 5.5$ T^2/m, conserved with reversed flow at $B\mathrm{d}B/\mathrm{d}z = 11$ T^2/m and is doubled and tripled at $B\mathrm{d}B/\mathrm{d}z = -5.5$ and -11 T^2/m, respectively. Consequently, Nu followed the evolution of Ra in accordance to Catton's correlation. The three-dimensional effect of the magnetic field gradient is significant only at very low Ra value when vertical magneto-gravity buoyancy is weak comparatively to the horizontal magnetic components.

Acknowledgment

The authors gratefully acknowledge Dr. K. Messadek for fruitful discussions.

References

[1] S. Chandrasekhar, Hydrodynamic and Hydromagnetic Stability, Clarendon Press, Oxford, 1961, pp. 146–195.

[2] B.A. Finlayson, Convective instability of ferromagnetic fluids, J. Fluid Mech. 40 (4) (1970) 753–767.

[3] L. Schwab, U. Hildebrandt, K. Stierstadt, Magnetic Bénard convection, J. Magn. Magn. Mater. 39 (1983) 113–114.

[4] M. Wanke, T. Voelker, J. Hilljegerdes, G. Coverdale, S. Odenbach, P. Fannin, G. den Dulk, G. Schaumburg, Thermal transport phenomena in magnetic fluids under microgravity conditions, in: Proceedings of the 10th International Conference on Magnetic Fluids, São Paulo, Brazil, August 2–6, 2004.

[5] D. Braithwaite, E. Beaugnon, R. Tournier, Magnetically controlled convection in a paramagnetic fluid, Nature 354 (1991) 7–8.

[6] J. Huang, D.D. Gray, B.F. Edwards, Thermoconvective instability of aramagnetic fluids in a non-uniform field, Phys. Rev. E 35 (1998) 5564–5571.

[7] J. Qi, N.I. Wakayama, A. Yabe, Magnetic control of thermal convection in electrically non-conducting or low-conducting paramagnetic fluids, Int. J. Heat Mass Transfer 44 (2001) 3043–3052.

[8] S. Maki, T. Tagawa, H. Ozoe, Enhanced convection or quasi-conduction states measured in a super-conducting magnet for air in a vertical cylindrical enclosure heated from below and cooled from above in a gravity field, J. Heat Transfer 124 (2002) 667–673.

[9] J.R. Carruthers, R. Wolfe, Magnetothermal convection in insulating paramagnetic fluids, J. Appl. Phys. 39 (12) (1968) 5718–5722.

[10] C.D. Seybert, J.W. Evans, F. Lesie, W.K. Jones Jr., Suppression/reversal of natural convection by exploiting the temperature composition dependence of magnetic susceptibility, J. Appl. Phys. 88 (7) (2000) 4347–4351.

[11] T. Tagawa, R. Shigemitsu, H. Ozoe, Magnetizing force modelled and numerically solved for natural convection of air in a cubic enclosure: effect of the direction of the magnetic field, Int. J. Heat Mass Transfer 45 (2002) 267–277.

[12] L.K. Urankar, Vector potential and magnetic field of current-carrying finite arc segment in analytical form, IEEE Trans. Magn. 18 (6) (1982) 1860–1866.

[13] Fluent 6.01, User's guide, 2002.

[14] A.E. Gill, Boundary-layer regime for convection in a rectangular cavity, J. Fluid Mech. 26 (3) (1966) 515–536.

[15] G.D. McBain, Fully developed laminar buoyant flow in vertical cavities and ducts of bounded section, J. Fluid Mech. 401 (1999) 365–377.

[16] I. Catton, Natural convection in enclosures, in: Proceedings of the Sixth International Heat Transfer Conference 6 (1978) 13–31.